

In Situ Detection of Interplanetary and Jovian Nanodust with Radio and Plasma Wave Instruments

Nicole Meyer-Vernet and Arnaud Zaslavsky

Abstract Radio and plasma wave instruments in space can detect cosmic dust over a wide range of sizes via impact ionisation. Such measurements were performed on a number of spacecraft in various environments, using instruments that were generally not designed to do so, and have been recently extended to nanodust. The technique is based on analysis of the electric pulses induced by the plasma clouds produced by impact ionisation of fast dust particles. Nanodust can be detected in this way despite their small mass because (1) their large charge-to-mass ratio enables them to be accelerated to high speeds, and (2) the amplitude of the induced electric pulses increases much faster with speed than with mass. As a result, the impacts of nanodust produce signals as high as those of larger and slower grains. This chapter describes the basic principles of such measurements, the underlying physics, the applications to the recent discovery of interplanetary nanodust near Earth orbit with STEREO/WAVES, and to the detection of Jovian nanodust with Cassini/RPWS. Finally, we give some perspectives for wave instruments as dust detectors.

1 Introduction

Even though this was not immediately recognised, the first in situ detection of fast nanodust in space took place 20 years ago, when the Ulysses cosmic dust analyser detected streams of particles ejected by Jupiter that were initially identified as 0.2- μm grains moving at about 50 km/s (Grün et al. 1992). A few years later, these streams were recognised as made instead of fast nanodust, $\sim 10^3$ times less massive and moving 5–10 times faster than previously reported, i.e., outside the calibration range of the instrument (Zook et al. 1996). This pioneering result opened the way to

N. Meyer-Vernet (✉) · A. Zaslavsky

LESIA - Observatoire de Paris, CNRS, UPMC, Université Paris Diderot, 92190 Meudon, France
e-mail: nicole.meyer@obspm.fr; arnaud.zaslavsky@obspm.fr

extensive studies of nanodust produced by outer planets' satellites and rings, whose electric charge enables them to be ejected by the electric field of the corotating magnetosphere and further accelerated by the magnetised solar wind (Johnson et al. 1980; Horányi et al. 1997; Hsu et al. 2012).

That nanodust could also be produced in the inner heliosphere and be accelerated to high speeds by the solar wind was suggested a few years ago (Mann et al. 2007). Nevertheless, when the STEREO/WAVES instrument detected serendipitously voltage pulses of amplitude corresponding to impacts of such fast nanodust, with a rate similar to that expected from extrapolation of the interplanetary dust model (Meyer-Vernet et al. 2009a), this came as a surprise since conventional dust detectors had not detected such interplanetary nanodust (Grün et al. 2001).

In fact, this capability of wave instruments to measure dust should not have been surprising since nearly 30 years ago, the first in situ measurement of microdust in the E and G rings of Saturn was performed serendipitously by the radio (Aubier et al. 1983) and the plasma wave (Gurnett et al. 1983) instruments on the spacecraft Voyager, despite the fact that neither the radio (Warwick et al. 1982) nor the plasma wave (Scarf et al. 1982) instrument was designed to do so. These pioneering results opened the way to microdust measurements with wave instruments in various environments, including other planetary environments and comets (see reviews by Oberc 1996; Meyer-Vernet 2001).

The capability of wave experiments to measure nanodust was confirmed by the detection of nanodust near Jupiter by the Cassini/RPWS instrument (Meyer-Vernet et al. 2009b), and the STEREO pioneering result was subsequently confirmed and expanded by a detailed analysis based on an independent dataset acquired by a different subsystem of the STEREO/WAVES instrument (Zaslavsky et al. 2012). On the theoretical front, detailed calculations of the nanodust dynamics confirmed their ejection from the inner heliosphere and their acceleration in the solar wind to several hundred of kilometres per second at 1 AU (Czechowski and Mann 2010).

In this chapter, we summarise the basic principles of dust detection with a wave instrument and their extension to nanodust (Sect. 2), and the main results obtained for interplanetary nanodust near 1 AU with STEREO (Sect. 3), and for Jovian nanodust with Cassini (Sect. 4). In Sect. 5, we give some perspectives for wave instruments, which are complementary to traditional dust detectors since they have a much greater collecting area and are much less reliant on a specific spacecraft attitude. Unless otherwise stated, we use the International System of units.

2 Basics of In Situ Dust Detection with a Wave Instrument

The traditional use of wave instruments is the observation of electromagnetic waves, whose propagation from large distances enables measurements of distant objects by radio techniques. It was soon realised that these instruments could also be used at lower frequencies for in situ measurements, by detecting intense plasma waves produced by instabilities. A crucial step was reached by showing that, since

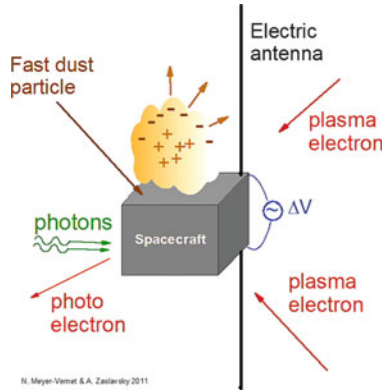


Fig. 1 Principle of in situ measurements of plasma and dust with a wave instrument. Plasma particles passing-by the antennas (as well as impacting and ejected particles) produce a quasi-thermal electrostatic noise whose power spectrum reveals the plasma density, temperature, and other properties. Dust impacts at fast speed produce partial ionisation of the dust and target, yielding an expanding plasma cloud. This produces voltage pulses whose analysis reveals some dust properties

electrostatic waves are closely coupled to plasma particles, a sensitive wave receiver in space can also measure in situ several bulk properties of *stable* plasmas (Meyer-Vernet 1979). This is because the motion of the charged particles around the antenna, as well as the impacts or emission (Fig. 1), produces a quasi-thermal noise whose analysis reveals their density, temperature, and possible nonthermal properties. This has led to the technique of quasi-thermal noise spectroscopy, which has been successfully used for plasma measurements in various space environments (Meyer-Vernet et al. 1998).

But electric antennas are not only sensitive and accurate plasma detectors of equivalent cross-section much greater than their physical size. They can also detect dust, since impacts of high speed dust particles vaporise and partially ionise them as well as some material of the impact craters, producing plasma clouds whose electric field reveals some dust properties. As a result, electric antennas can also be used as sensitive dust detectors of large detecting area since it may be the whole spacecraft surface.

2.1 What Do Radio and Plasma Wave Instruments Detect

Wave instruments used for in situ measurements of plasma and dust deliver a voltage¹ using two basic systems:

¹We do not consider here magnetic field measurements.

- Electric antennas made of conductive booms,² which are used in two main ways:
 - In monopole mode, the voltage is measured between one antenna boom and the spacecraft conductive structure.
 - In dipole mode, the voltage is measured between two antenna booms.
- Electronic analysers which transform the signal into quantities suitable for analysis, and deliver two main types of data:
 - Time-integrated power spectra, equivalent to Fourier transforms of the auto-correlation function of the measured voltage; this part of the instrument is called a frequency receiver.
 - Broadband voltage waveforms made of time series data captured at a very high rate; this part of the instrument is called a time domain sampler (TDS).

The power spectrum delivered by frequency receivers corresponds to

$$V_f^2 = 2 \int_{-\infty}^{+\infty} d\tau e^{i\omega\tau} \langle V(t)V(t + \tau) \rangle \quad (1)$$

(where the frequency $f = \omega/2\pi$). Since this involves a time integration, frequency receivers are not adapted to study short individual events, even though in modern instruments such as STEREO/WAVES and the high-frequency (hf) receiver of Cassini/RPWS, the integration is calculated over short times (typically <1 s). Furthermore, in order to cover a large dynamic range, the STEREO low-frequency receiver (LFR) is equipped with an automatic gain control (AGC) which adjusts the gain according to the input level; an adequate response thus requires the signal to be stationary or to be made of a large number of individual events during the acquisition time. In contrast, TDSs are adapted to study individual events since the time series are rather long (typically 131 ms on STEREO) and acquired at a very high rate (typically $8 \mu\text{s}$ on STEREO). However, they involve so huge a quantity of data that a selection of the telemetered periods must be made on board; in complement, other types of data are telemetered as for example the peak signal within some given time periods, or histograms (Bougeret et al. 2008).

Figure 2 shows an example of spectrograms acquired by the low and high frequency receivers on STEREO A and B. The spectra are displayed as frequency vs. time with relative intensity above background (in dB) scaled in grey. They show solar type III bursts—a type of solar emission for the study of which the instrument was designed, and unexpected voltage pulses attributed to nanodust impacts that will be discussed in Sect. 2.3. Likewise, the TDS was designed to study Langmuir wave packets as the one shown in Fig. 3 or other types of plasma instabilities, but

²We do not consider antennas made of spheres because they must be mounted on booms, which complicates considerably the analysis (Manning, 1998), so that they are rarely used.

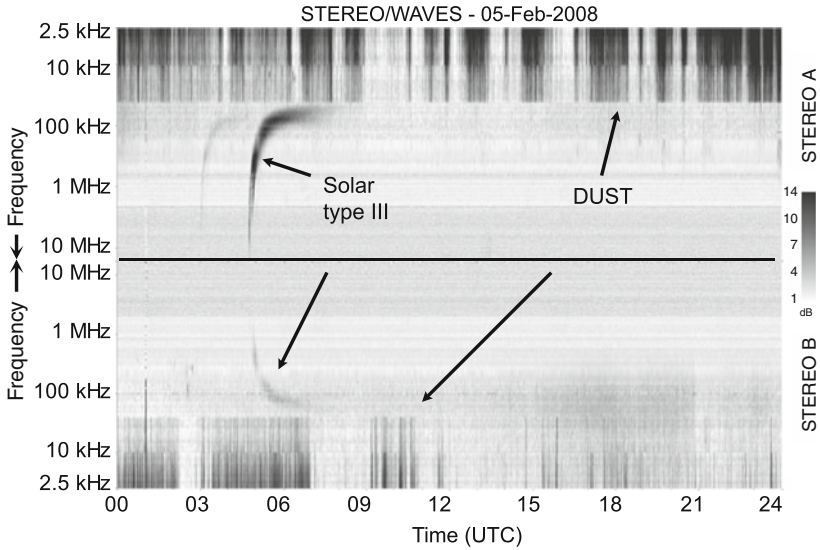


Fig. 2 Typical spectrograms displayed as frequency (2.5 kHz–20 MHz) vs. time (24 h) with relative intensity scaled in *grey*, from the low and high frequency receivers with the X–Y dipole on STEREO A and B (then separated by 45° longitude), showing solar type III bursts and voltage pulses produced by nanodust impacts. The discontinuities between frequency bands are due to differences in integration times. Both spacecraft see the same solar type III, albeit with different intensities, due to the directivity of the source of electromagnetic waves and to scattering by coronal and solar wind plasma. In contrast, they see different dust pulses since the measurement is local

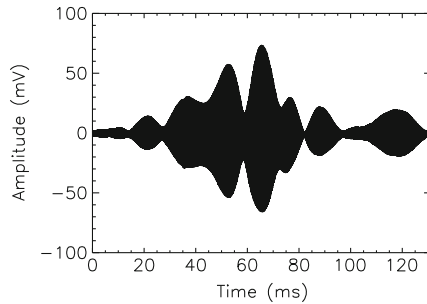


Fig. 3 Voltage waveform from the TDS measured on 31:01:2007 with the STEREO B/X-antenna, showing a Langmuir wave packet

it turned out to measure voltage pulses as shown in Fig. 7 that will be discussed in Sect. 2.3.

Since the detection of dust by wave instruments builds on many concepts introduced for plasma detection, we first remind them briefly.

2.2 *How Do Passive Wave Instruments Measure the Ambient Plasma*

A stable plasma is characterised by the velocity distributions of the particle species, whose quasi-thermal motion produces electric field fluctuations entirely determined by these velocity distributions. On the other hand, an electric antenna is characterised by its current distribution, which is determined by its geometry for a short dipole (of half-length $L \ll \lambda$, the wavelength). As a result, the voltage power spectral density at the ports of a given electric antenna can be theoretically calculated as a function of the plasma properties, so that these properties can be deduced from spectroscopy of the power measured by a frequency receiver.

For timescales smaller than the inverse of the plasma frequency ($f_p \propto n^{1/2}$, n being the ambient electron density), the electric field of a charged particle moving slower than the electron thermal speed v_{th} is screened at distances greater than the Debye length $L_D \propto (T/n)^{1/2}$ (T being the temperature). Thermal electrons moving within this distance from the antenna thus produce voltage pulses of timescale $\sim L_D/v_{th} \sim 1/2\pi f_p$. From the properties of Fourier transforms, this yields a flat noise spectrum at frequencies $< f_p$. On the other hand, faster charged particles (as well as some perturbations) produce Langmuir waves of frequencies $\simeq f_p$ and wavelengths $> L_D$ (~ 10 m in the solar wind). This produces a quasi-thermal noise spectral peak at f_p if the antenna length $L > L_D$.

Fitting the measured spectra to a theoretical calculation thus yields the electron density and temperature as well as other plasma properties, so that the electric antenna serves as a plasma detector of equivalent cross section $\sim 2L \times L_D$ —typically several hundred square metres in the solar wind, which generally exceeds the antenna physical cross section by more than three orders of magnitude. An additional contribution comes from electrons collected by the antenna surface (or ejected by it), which produce voltage pulses of rise time $\tau_e \sim \text{Min}(L, L_D)/v_{th}$ (decreasing at a much longer timescale); from the properties of Fourier transforms, this yields a power spectrum $\propto f^{-2}$ at frequencies $< 1/2\pi\tau_e$. Basic theoretical expressions and approximate analytical formulas are given by Meyer-Vernet and Perche (1989). Note that this plasma noise cannot be measured by TDSs since it involves the superposition of a huge number of extremely small signals.³

Finally, we note that the instantaneous voltage measured by each wire antenna boom shorter than the electromagnetic wavelength is equal to the average potential V_A along its length. However, the receiver of impedance Z_R detects $V_R = \Gamma V_A$, where $\Gamma = Z_R/(Z_R + Z_A) \simeq C_A/(C_A + C_{stray})$, since the impedances are mainly capacitive at the frequencies considered. The receiver impedance is essentially due to the stray capacitance C_{stray} , whereas the antenna impedance Z_A , mainly due to

³Each passing electron produces a voltage pulse of order of magnitude $e/4\pi\epsilon_0 L_D$ (where e is the electron charge), which amounts to $\sim 10^{-10}$ V in the solar wind at 1 AU. The number of such pulses per second $\sim 2n v_{th} L L_D > 2 \times 10^{15} \text{ s}^{-1}$ in the solar wind at 1 AU if $L > L_D$.

the antenna capacitance C_A , can be calculated from the plasma properties (Meyer-Vernet and Perche 1989).

2.3 *How Do Wave Instruments Measure the Ambient Dust Flux*

In situ measurements by wave instruments are based on the detection of electrostatic fields produced by electric charges. For dust grains, this may be the charge carried by the grains, or the much greater charge produced by high speed impact ionisation.

2.3.1 Nonimpacting Dust Grains

Dust particles in a plasma carry an electric charge due to photoelectron emission, collection of plasma particles, and secondary emission. Their motion thus produces electrostatic field variations, so that an electric antenna can in principle detect the noise produced by dust grains passing by the antenna (and/or collected by its surface). This noise can be observed with a frequency receiver if the dust charge and concentration are high enough (Meyer-Vernet 2001). Contrary to the plasma thermal noise, this “dust thermal noise” can also be observed with a sensitive TDS for highly charged dust grains, with an equivalent cross section $\sim 2L \times L_D$ —similar to that for plasma detection (typically $>200 \text{ m}^2$ in the solar wind), as proposed by Meuris et al. (1996).

However, when the dust grains move faster than a few km/s, the sound speed in bulk matter, another effect becomes dominant: impact ionisation.

2.3.2 Impact Ionisation

A dust grain impacting a solid target such as a spacecraft or its appendages produces a strong shock compression which vaporises and ionises the dust as well as some material of the impact crater. This material then expands into the low-pressure ambient medium, cooling and partially recombining (Drapatz and Michel, 1974). The residual ionisation of the expanding plasma cloudlet can be used to detect the grain. In practice, one measures the charge Q carried by the electrons and/or the ions by separating and recollecting them, and deduces the grain mass m and speed v from laboratory calibrations of the timescales of the signals (to deduce v), and of the relationship $Q(m, v)$ (to deduce m). This is the principle of classical impact ionisation dust detectors (Auer, 2001).

The relationship $Q(m, v)$ depends on the material of both the grain and the target as well as on the impact angle; despite extensive theoretical calculations and simulations (Kissel and Krüger 1987; Hornung and Kissel 1994), it remains largely

empirical (Krüger, 1996). In order of magnitude, we have $Q \propto m v^{3.5}$ (Dietzel et al. 1973), with a typical relationship

$$Q \simeq 0.7 m^{1.02} v^{3.48}, \quad (2)$$

with Q in Cb, m in kg, v in km s^{-1} (McBride and McDonnell, 1999). The three coefficients in (2) depend on mass, speed, angle of incidence, as well as grain and target composition (Göller and Grün 1989), so that Q may differ from this relationship by one order of magnitude.

An important consequence of (2) is that a 10-nm grain moving at 300 km/s in the solar wind, as predicted by dynamics (Mann et al. 2007; Czechowski and Mann 2012), should produce the same impact charge as a grain ~ 500 times more massive impacting at 50 km/s. Note, however, that such empirical relationships are based on simulations involving grains of mass greater than about 10^{-18} kg and speed smaller than about 80 km/s (Auer, 2001), i.e., outside the range of fast nanodust.

Some comparisons may be instructive. First, let us compare the amount of material involved in the charge Q given in (2) to that contained in the grain itself. The mass m_Q of the ions—assumed to be singly ionised—involved in Q is $A m_p Q / e$ (m_p being the proton mass and A the average ion atomic mass), so that

$$m_Q / m \simeq (A Q / m) (m_p / e) \sim 10^{-8} \times A m^{0.02} v^{3.48}, \quad (3)$$

For $v \simeq 300$ km/s, this yields $m_Q / m \sim A$ over the whole grain mass range, so that for $A > 1$ a significant part of the impact charge comes from the target's material.

Second, let us compare the mass m_{crater} involved in the impact crater to the grain mass m . From empirical expressions for dust impacts on various targets (McBride and McDonnell, 1999), we get

$$m_{\text{crater}} / m \sim m^{0.056} v^{2.42}, \quad (4)$$

in order of magnitude,⁴ with m in kg and v in km s^{-1} . This ratio exceeds unity in most practical cases. For a 10-nm grain ($m = 10^{-20}$ kg) impacting at $v = 300$ km/s, (4) yields $m_{\text{crater}} / m \sim 10^5$, i.e., the crater is of size nearly 1 μm . This means that most of the ejected mass comes from the target, presumably in the form of debris, and since (3) yields $m_Q / m \geq 1$, the total ejected mass m_{crater} exceeds by a large amount the ionised mass m_Q .

Third, let us compare the impact charge Q to the charge q carried by the dust grain itself before impact. For a grain of radius r , we have $q \simeq 4\pi\epsilon_0 r \Phi$, with $\Phi \simeq$

⁴The ejected mass is very dependent on the materials involved, and is expected to increase as the dynamic yield strength and the mass density of the target material decrease (Shanbing et al. 1994). For deriving (4), we have assumed a crater volume $\sim \epsilon^3$, where ϵ is the penetration distance, a target yield stress of the same order of magnitude as that of aluminium, and a mass density $\sim 2.5 \times 10^3$ kg m^{-3} for the target and the grain.

5–10 V in the interplanetary medium (see for example [Meyer-Vernet 2007](#)). With a grain mass density of $2.5 \times 10^3 \text{ kg m}^{-3}$, this yields

$$Q/q \sim 2 \times 10^{10} m^{0.69} v^{3.48}, \quad (5)$$

so that $Q/q \gg 1$ in almost all practical cases. Hence, for dust grains of impact speed greater than a few km/s, impact ionisation is generally the dominant mechanism for detection by wave instruments. For a 10-nm grain impacting at 300 km/s, (5) yields $Q/q \sim 10^5$.

However, in the absence of laboratory simulations and calculations for fast nanodust, the reliability of (2), as well as (3)–(5), for such particles remains open to question. Surface effects play an increasing role as size decreases; for example in a 1-nm grain, a significant proportion of the atoms lie at the surface. Furthermore, since the ejected neutral material, in the form of solid or liquid debris and/or gases, exceeds considerably the ionised material, it may affect the evolution of the system. The expected disintegration of the liquid phase into a large number of small droplets before vaporisation, complicates considerably the simulation ([Hornung et al. 2000](#)). These difficulties are especially important in the case of STEREO since detailed data on the material of the blankets covering the spacecraft are not easily available, and the published spacecraft description ([Driesman et al. 2008](#)) contains errors in the technical properties of the blankets. Finally, energy conservation yields a speed limit for (2) to hold. Since the energy required to produce free charges by vaporisation and ionisation, $\simeq 10 \text{ eV}$ for each of the Q/e ions, cannot exceed the grain kinetic energy,⁵ the validity of (2) requires at least $v < 2 \times 10^3 \text{ km/s}$.

Be that as it may, it is noteworthy that the initial identification of Jovian dust streams by traditional detectors, which was based on their calibration, has been subsequently modified from dynamical arguments by multiplying the mass by 10^{-3} and the speed by 5–10 ([Zook et al. 1996](#)). Since $10^{-3} \simeq 7^{-3.5}$, this suggests that the $Q \propto m v^{3.5}$ law still holds for these grains.

Finally, let us note that a fast nanodust impact represents a huge incident power since for a grain of radius r and mass density ρ , the incident kinetic energy $\rho(4\pi r^3/3)v^2/2$ comes over the surface $\sim \pi r^2$ during a time $\sim r/v$, which yields a power $P \sim \rho v^3$. For $\rho \sim 2.5 \times 10^3 \text{ kg m}^{-3}$ and $v \sim 300 \text{ km/s}$, this yields $P \sim 10^{20} \text{ W/m}^2$ —a huge power, greater by several orders of magnitude than that involved in laboratory simulations.

2.3.3 The Impact Plasma Cloud

Let us study the properties of the plasma cloud in the simple case when it behaves independently of its environment. This is expected to hold when two conditions

⁵The actual limit is expected to be smaller since part of the energy is also used for vaporisation, formation of debris, and kinetic energy of the expelled material.

are met: first its density should significantly exceed that of the surrounding plasma; second, the energy of its particles (in eV) should significantly exceed the electric potential of the spacecraft and antennas. We also neglect the neutral gas component of the impact plasma cloud as well as the solid or liquid debris, and assume that the cloud contains Q/e ions (singly ionised positively) and the same number of electrons, is uniform, of spherical shape, and expanding at constant speed v_E . As the radius increases with time t as $R \sim v_E t$, the electron number density decreases as $n \simeq 3Q/(4\pi R^3 e) \propto t^{-3}$. The maximum radius R_{\max} and lifetime t_{\max} of the cloud are reached when its electron density has decreased to the ambient value n_a , i.e.

$$R_{\max} \sim (3Q/4\pi e n_a)^{1/3}, \quad (6)$$

$$t_{\max} \sim R_{\max}/v_E. \quad (7)$$

An important quantity is the ratio between the cloud's proper Debye length $L_D \propto (T/n)^{1/2}$ and its radius R , which controls charge separation

$$L_D/R \simeq \left(\frac{4\pi\epsilon_0 R T_{(\text{eV})}}{3Q} \right)^{1/2}. \quad (8)$$

If $L_D/R \ll 1$, the cloud is quasi-neutral except in a small outer shell of width L_D which contains a charge $\sim Q \times L_D/R$ producing an electric potential

$$\phi_c \sim (QL_D/R)/4\pi\epsilon_0 R. \quad (9)$$

The evolution of the cloud's temperature T as it expands depends on its collisional state. The electron and ion mean free path is determined by Coulomb collisions, whose effective cross section is determined by the radius r_L at which the Coulomb potential of a plasma particle $\sim e/4\pi\epsilon_0 r_L$ equals its kinetic energy $\propto T$; this yields a free path $\propto T^2$; taking into account large distance particle encounters up to distance L_D increases the effective cross section by a factor $\lambda_0 = \ln(L_D/r_L)$. The cloud's electrons and ions become collisionally decoupled when the mean free path becomes greater than the cloud's radius, which therefore takes place when the radius is equal to $R_0 \simeq (e/4\pi\epsilon_0 T_{0(\text{eV})})(3\lambda_0 Q/4e)^{1/2}$ (Pantellini et al. 2012a). Here $T_{0(\text{eV})} = k_B T_0/e$ where T_0 is the temperature of the cloud at this time, and λ_0 lies typically between 2 and 10. One deduces from (8) that at the beginning of the collisionless regime $L_{D0}/R_0 \simeq (\lambda_0 e/12Q)^{1/4} \ll 1$ since $Q/e \gg 1$ and $\lambda_0 > 1$.

This problem has been recently studied by Pantellini et al. (2012a) with a N-body simulation. As the cloud expands, the problem becomes self-similar, so that the ratio L_D/R remains constant; therefore, according to (8), the electron temperature decreases⁶ as $T \propto 1/R$. An important consequence is that since $L_{D0}/R_0 \ll 1$, we

⁶This can be understood as follows. Since most of the electrons are trapped in the cloud, we have $T_{(\text{eV})} \sim \phi_c$, the cloud's potential. Since $L_D \propto (T/n)^{1/2}$ and $n \propto R^{-3}$, we have

also have from (8) $L_D/R \ll 1$ during the collisionless expansion, i.e., the cloud is quasi-neutral at collisional decoupling and remains so as it expands further. For a 10-nm grain impacting at 300 km/s in the solar wind at 1 AU where $n_a \sim 5 \times 10^6 \text{ m}^{-3}$, (2) and (6) yield $Q \sim 10^{-12} \text{ C}$ and $R_{\text{max}} \sim 1 \text{ m}$, so that $R_0 \sim 10^{-5}/T_{0(\text{eV})}$, $L_D/R \sim 0.02$, and $\phi_c \sim 2 \times 10^{-4} \text{ V}$ at distance R_{max} . Therefore the collisionless regime starts at a very small value of the cloud's radius, the cloud is quasi-neutral except in a thin outer shell, and it produces a very small electric potential (Pantellini et al. 2012a).

2.3.4 Application to Wave Instruments

The charge in the expanding impact plasma cloud can in principle be detected by wave instruments in a number of ways:

1. Direct recollection of the cloud's charges by the spacecraft or antennas (Aubier et al. 1983; Meyer-Vernet 1985).
2. Perturbation of the current balance of the spacecraft or antennas (Oberc et al. 1990).
3. Direct detection of the electrostatic field produced by charge separation in the impact plasma cloud (Oberc 1994, 1996).
4. Detection of electromagnetic radiation produced by charge oscillations in the plasma cloud (Foschini 1998).

Direct Charge Recollection

In the solar wind, the floating potential of the spacecraft and antennas is mainly determined by the balance of photoelectron emission and collection of ambient electrons. Since an uncharged surface generally ejects many more photoelectrons than it collects ambient solar wind electrons (whereas ambient ions contribute much less), the equilibrium potential is positive and of the order of magnitude of a few times the photoelectron temperature expressed in eV, $T_{\text{ph}} \sim 3 \text{ eV}$, i.e. $\Phi \sim 5\text{--}10 \text{ V}$, in order to bind the photoelectrons sufficiently to make their flux balance that of the ambient electrons. For nanodust, R_{max} is much smaller than the solar wind Debye length,⁷ and of the order of magnitude of the Debye length of the photoelectrons ejected by the sunlit surfaces.⁸ Hence the impact plasma cloud lies in the electric field produced by the spacecraft charge. Since the spacecraft (or

$\phi_c \propto (T/R)^{1/2}$, whence from (9) $T \simeq 1/R$. In contrast, an adiabatic behaviour would yield instead $T \propto n^{2/3} \propto R^{-2}$.

⁷The solar wind density $n_a \sim 5 \times 10^6 \text{ m}^{-3} \propto d^{-2}$, so that from (6) $R_{\text{max}} \propto d^{2/3}$, and $L_{\text{Da}} \simeq 10 \times d^\alpha \text{ m}$ where d is the heliocentric distance in AU and $1/2 < \alpha < 1$ (Meyer-Vernet 2007). Hence, $L_{\text{Da}}/R_{\text{max}} \sim 10$ for $Q \sim 10^{-12} \text{ C}$, with a variation as $Q^{-1/3}$ and a weak variation with d .

⁸With an ejected photoelectron current $I_{\text{ph0}} \simeq 5 \times 10^{-5} \text{ Am}^{-2}$ and $T_{\text{ph}} \simeq 3 \text{ eV}$, the photoelectron Debye length $L_{\text{Dph}} \simeq (\epsilon_0/I_{\text{ph0}})^{1/2}(T_{\text{ph(eV)}})^{3/4}(e/m_e)^{1/4} \sim 1 \text{ m}$ at 1 AU, with $L_{\text{Dph}} \propto d$ (Meyer-Vernet 2007).

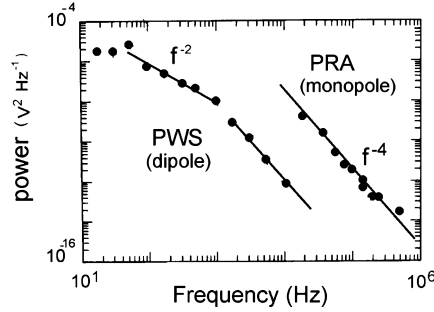


Fig. 4 Voltage power spectrum measured in Saturn G ring by the (high frequency) radio (PRA) and (lower frequency) plasma wave (PWS) instruments on Voyager 2, with respectively monopole and dipole antennas. At similar frequencies, the power is higher by four orders of magnitude on the monopole than on the dipole. Adapted from [Mann et al. \(2011\)](#)

antenna) electric potential is much greater than the small potential of the quasi-neutral cloud estimated in Sect. 2.3.3, and exceeds the kinetic energy (in eV) of the cloud’s electrons, they are easily recollected. The spacecraft receives most of the dust impacts and of the recollected electrons because of its larger cross section compared to the antenna, so that an impact makes its voltage vary by $-Q/C_{sc}$, C_{sc} being the spacecraft capacitance.

Each monopole sees the difference between its own voltage (which barely changes except if the impact takes place close to it—see item 2) and that of the spacecraft. Therefore, each impact produces by this mechanism a *positive* voltage pulse of similar amplitude on all the *monopole* antennas, i.e., taking the receiver gain into account

$$\delta V_1 \sim \Gamma Q / C_{sc}. \quad (10)$$

On the other hand, since a dipole antenna sees the difference in voltage between two monopoles, it detects a much smaller signal, produced by circuit imbalances (the so-called common-mode rejection) and/or by weak recollection by the antennas themselves. This difficulty in calibrating the dipole mode for direct charge recollection is at the origin of the conflicting results obtained on Voyager in planetary rings by the radio ([Aubier et al. 1983](#)) and the plasma wave ([Gurnett et al. 1983](#)) instruments, which used respectively monopole and dipole configurations (see Fig. 4 and discussions by [Oberc 1994](#); [Meyer-Vernet 1985, 2001](#)).

The impact voltage pulse has a short rise time τ_r determined by collection of the cloud’s electrons, and a much longer decay time τ_d , determined by the discharge of the spacecraft via the ambient plasma and photoelectron currents. Such a pulse has the generic squared Fourier transform ([Meyer-Vernet 1985](#))

$$V_{f(\text{pulse})}^2 \simeq \frac{2\delta V^2 / \omega^2}{(1 + \omega^2 \tau_r^2)(1 + 1/\omega^2 \tau_d^2)}. \quad (11)$$

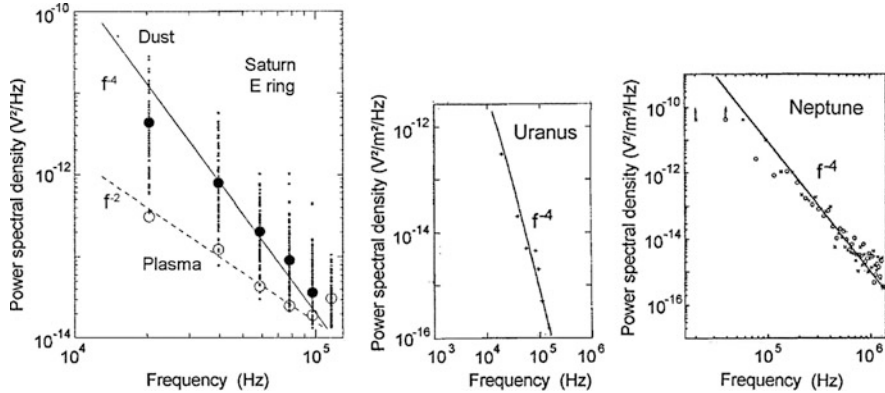


Fig. 5 Voltage power spectral density measured by the monopole antennas on Voyager/PRA (Warwick et al. 1982) in the microdust rings of Saturn (adapted from Meyer-Vernet et al. 1996), Uranus (adapted from Meyer-Vernet et al. 1986), and Neptune (adapted from Pedersen et al. 1991)

Here $\delta V \equiv \delta V_1$. At frequencies $f = \omega/2\pi \gg 1/2\pi\tau_r \gg 1/2\pi\tau_d$, (11) yields $V_f^2 \propto f^{-4}$, as consistently observed at high frequencies in the presence of dust impacts, whereas the slope decreases at lower frequencies (Figs. 4, 5, 8, and 12).

Equation (11) must be integrated over the mass distribution of the dust impact rate, which yields

$$V_f^2 \simeq \int dm V_{(\text{pulse})}^2 S(m) dF/dm \tag{12}$$

where $F(m)$ is the cumulative dust flux and $S(m)$ the surface involved, which for this mechanism is the spacecraft area subjected to impacts.

For fast nanodust, we have seen that Q is of the order of magnitude of 10^{-12} C or smaller, so that with the typical spacecraft⁹ capacitance $C_{sc} \simeq 200$ pF and $\Gamma \simeq 0.5$, the pulse amplitude is $\delta V_1 \sim \Gamma Q/C_{sc} \simeq 2.5$ mV. Such a small signal requires a sensitive TDS receiver to be detected individually. On the other hand, the impacts can be observed with a frequency receiver if the impact rate is very high; we will show an application for nanodust detection near Jupiter with Cassini/RPWS in Sect. 4. Hence, other mechanisms may dominate the signal.

Perturbation of the Current Balance of the Spacecraft or Antennas

As we already noted, the floating potential of a surface in the interplanetary medium is mainly determined by balance between the photoelectron and ambient electron

⁹These typical values of C_{sc} and Γ hold for both STEREO/WAVES (Bale et al. 2008; Zaslavsky et al. 2011, 2012) and Cassini/RPWS (Gurnett et al. 2004; Meyer-Vernet et al. 2009b).

currents. Let $I_{\text{ph}0}$ and I_{e0} be respectively the photo and ambient electron currents per unit surface at zero potential, and $T_{\text{ph}(eV)}$ and $T_{e(eV)}$ the corresponding electron temperatures in eV. A surface at equilibrium potential $\Phi > 0$ attracts the ejected photoelectrons so that only a fraction $I_{\text{ph}}/I_{\text{ph}0} \simeq (1 + \Phi/T_{\text{ph}(eV)})^\alpha \exp(-\Phi/T_{\text{ph}(eV)})$ does not return, whereas the attracted ambient electron current becomes $I_e \simeq I_{e0}(1 + \Phi/T_{e(eV)})^\alpha$, with $\alpha = (n - 1)/2$ in n -dimensional geometry¹⁰ (Meyer-Vernet 2007). Hence, since in the solar wind $I_{\text{ph}0} \gg I_{e0}$ and $T_e \gg T_{\text{ph}}$, the equilibrium potential is $\Phi \sim T_{\text{ph}(eV)} \ln(I_{\text{ph}0}/I_{e0})$, and any significant perturbation will change this potential by a value of the order of magnitude of $T_{\text{ph}(eV)}$.

Depending on the impact charge, on the photoelectron current, and on the surfaces involved, this may affect the spacecraft and/or the electric antennas. A large grain producing an impact plasma cloud that engulfs the spacecraft may perturb its current balance, which can mainly be observed in monopole mode. In contrast, a fast nanodust impact producing a smaller impact plasma cloud may disturb the equilibrium potential of an antenna affected by this tiny cloud, which can be observed in both dipole and monopole mode.

In particular, if a perturbation disturbs the photoelectrons ejected by an antenna so that a significant fraction of them do not return, the antenna potential will increase by $\delta V \sim T_{\text{ph}(eV)}$ if the perturbation holds during a large enough time. Such an effect was studied by Oberc et al. (1990) to interpret large voltage pulses observed by the Vega two plasma wave (APV-N) instrument in the dust coma of comet Halley, due to impacts of small particles yielding a charge $Q < 2 \times 10^{-12}$ C and producing voltage pulses much higher than the value (10) expected from electron recollection.

For a fast dust impact on a spacecraft, where a fraction x/L of an antenna is affected, the voltage pulse amplitude at the receiver ports is thus expected to be

$$\delta V_x \simeq \Gamma T_{\text{ph}(eV)} x/L, \quad (13)$$

if two conditions are met. First the electric potential perturbation produced by the impact cloud must prevent most of the photoelectrons ejected by the antenna to return to it. One might think naively that this requires the cloud's potential to be of the order of magnitude of the photoelectron energy (in eV). As shown by Pantellini et al. (2012b), this is not so because most of the photoelectrons returning to the antenna do so on elliptic trajectories of high eccentricity, and due to angular momentum conservation, the kinetic energy corresponding to their azimuthal velocity decreases as the square of the radial distance to the antenna axis. Since in the solar wind the photoelectron Debye length is much greater than the antenna radius a , most of the photoelectrons whose trajectory returns to the antenna lie far from its surface and thus have a very small azimuthal kinetic energy. Hence,

¹⁰For a spacecraft in the solar wind, of size generally greater (respectively, smaller) than the photo (respectively, plasma) electron Debye length, we have $\alpha = 0$ for I_{ph} , and $\alpha = 1$ for I_e . For a cylindrical antenna of radius (respectively, length) smaller (respectively, greater) than the Debye lengths, we have $\alpha = 1/2$.

a very small cloud's potential should be sufficient to increase significantly their azimuthal velocity and put them on less eccentric orbits that no longer cross the antenna. The second condition for (13) to hold is that the photoelectron current ejected by the antenna length x affected by the plasma cloud, $I_{\text{ph0}} \times 2ax$, must be able to eject the charge $C_A \delta V_x / \Gamma$ during the time available τ (which cannot exceed the lifetime (7) of the impact plasma cloud).¹¹ Here $C_A \simeq 2\pi\epsilon_0 L / \ln(L_{\text{Da}}/a)$ is the low-frequency capacitance of a monopole antenna of radius a and length L in the ambient plasma of Debye length L_{Da} (Meyer-Vernet and Perche 1989). From (13) this requires

$$I_{\text{ph0}} \geq \pi\epsilon_0 T_{\text{ph(eV)}} / [a\tau \ln(L_{\text{Da}}/a)]. \quad (14)$$

We shall see that this condition holds for STEREO at 1 AU (Sect. 4), but not for Cassini at 5 AU (Sect. 5) where the photoelectron current I_{ph0} is smaller by a factor of 25.

Integrating (13) over the probability of impacts at a given distance from an antenna on a spacecraft face of size $R_{\text{sc}} > R_{\text{max}}$ with a simplified model, one finds the average voltage pulse produced by a plasma cloud of maximum radius R_{max} (Zaslavsky et al. 2012) $\delta V_2 = \langle \delta V_x \rangle \simeq 2\Gamma T_{\text{ph(eV)}} R_{\text{max}}^3 / [3LR_{\text{sc}}^2]$. Substituting the value of R_{max} given in (6), this yields

$$\delta V_2 \simeq \frac{\Gamma T_{\text{ph(eV)}} Q}{2\pi e n_a L R_{\text{sc}}^2}. \quad (15)$$

For typical spacecraft and solar wind properties, (10) and (15) yield $\delta V_2 \gg \delta V_1$ at heliocentric distances > 0.3 AU, so that upon a nanodust impact on the spacecraft producing Q , the monopole whose photoelectrons are affected by the cloudlet should record a pulse of average amplitude $\delta V_2 + \delta V_1 \simeq \delta V_2$ given by (15), whereas the other monopoles should record simultaneously a pulse δV_1 given by (10) of much smaller amplitude, due to electron recollection by the spacecraft. An example measured on STEREO will be displayed in Sect. 3 (Fig. 9).

Charge Separation in the Cloud

From Sect. 2.3.3 and recent kinetic simulations with a N-body scheme (Pantellini et al. 2012a), the electrostatic field produced by charge separation in the impact plasma cloud is expected to be very small for nanodust impacts, so that this mechanism is not expected to be relevant for nanodust wave detection.

¹¹From (6) and (2) and a cloud's expanding speed $v_E \sim 20$ km/s, t_{max} is of order $30 \mu\text{s}$ for a 10-nm grain impact at 300 km/s producing $Q \simeq 10^{-12}$ C.

Electromagnetic Radiation

Plasma oscillations in the impact plasma cloud have been suggested to produce electromagnetic interference at high frequencies (Foschini 1998), and to generate transient magnetic fields (Stamper et al. 1971; Bird et al. 1973). For nanodust in the solar wind, Langmuir waves in the impact plasma cloud do not contribute to the observed spectral density since the frequencies involved are smaller than the plasma frequency in the cloud. The fast motion of the charges might also produce acoustic waves. However, the shape of the observed pulses (Fig. 9 in Sect. 3), as well as that of the observed spectrum (Fig. 8 in Sect. 3), which is close to the spectrum predicted by (11), suggest that this mechanism is not observed in our data.

3 Measurement of Interplanetary Nanodust with STEREO

The STEREO mission consists of two spacecraft in orbit at about 1 AU from the Sun, which, respectively, lead (STEREO A) and trail (STEREO B) the Earth, at heliolongitudes increasing by 22° /year. The WAVES instrument measures electric voltages as described in Sect. 2.1 with three orthogonal antennas of length $L = 6$ m (Bale et al. 2008).

Even though this mission was primarily designed to study the solar and inner heliospheric plasmas in three dimensions, it turned out to be a serendipitous dust detector over a wide range of sizes. Dust grains above several microns are detected by the Heliospheric Imagers in two ways: impacts on the spacecraft blankets produce trails of debris that are imaged by the cameras (St. Cyr et al. 2009), whereas direct impacts on the HI instruments themselves produce pointing offsets (Davis et al. 2012). These impacts are detected simultaneously by the WAVES instrument since they produce large voltage pulses that saturate TDS on the three antennas (St. Cyr et al. 2009). Indeed, a $1\text{-}\mu\text{m}$ radius grain of mass density $2.5 \times 10^3 \text{ kg m}^{-3}$ impacting at 20 km/s should produce from (2) and (10) a pulse due to charge recollection $\delta V_1 \sim 0.3 \text{ V}$ on the three antennas, which exceeds the instrument saturation level.

Concerning smaller sizes, the TDS instrument detects beta-meteoroids accelerated by the solar radiation pressure¹² to many tens of km/s (Mann et al. 2010) and interstellar dust of a few tenths micron impacting the spacecraft at several tens km/s (Zaslavsky et al. 2012), which all produce simultaneous pulses on the three antennas via direct charge recollection (10).

¹²The importance of radiation pressure is characterised by the ratio of this force to the solar gravitational force—called β , which has led to the name of the so-called beta-particles which are ejected by radiation pressure. Radiation pressure is negligible for nanodust since their size is much smaller than the radiation wavelength.

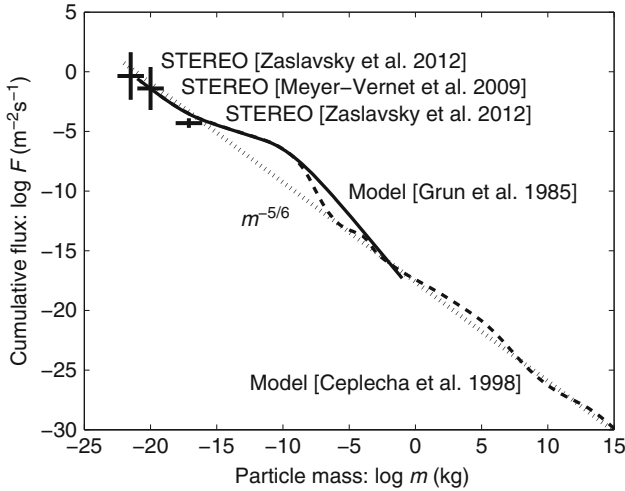
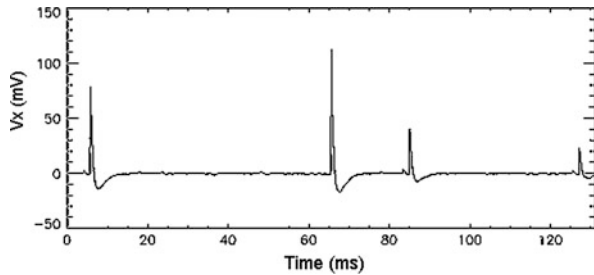


Fig. 6 Cumulative flux of interplanetary dust and bodies at 1 AU. The superposition of models for dust from Grün et al. (1985) (*continuous line*), small bodies from Ceplecha et al. (1998) (*dashed*), and collisional equilibrium $\propto m^{-5/6}$ (*dotted*), is reproduced from Meyer-Vernet (2007), with measurements of nanodust by Meyer-Vernet et al. (2009a) and of both nanodust and beta meteoroids by Zaslavsky et al. (2012) superimposed

Fig. 7 Sample of voltage on the X monopole of STEREO A during 131 ms, acquired by TDS on the same day as the spectrum of Fig. 8 (3 min before). The recoil is produced by instrumental filtering



However, as predicted by the increase in flux with decreasing mass of the interplanetary dust model (Fig. 6), by far the most frequent observed events are those we interpret as impacts of fast interplanetary nanodust on the spacecraft. As we have seen in Sect. 2.3.4, they produce a very small voltage on the three antennas via direct charge recollection, so that they are mainly detected on the antenna that is directly affected by the impact plasma cloud, via perturbation of the current balance (15), producing large pulses on TDS (Fig. 7) and characteristic f^{-4} spectra on LFR (Fig. 8).

The conspicuous nature of these events, which often dominate the spectrograms (see Fig. 2), enabled to discover these particles and to derive from the measured LFR power spectral density a preliminary order of magnitude estimate of the cumulative flux $\sim 4 \times 10^{-2} \text{ m}^{-2} \text{ s}^{-1}$ for $m \sim 10^{-20} \text{ kg}$, i.e., radius $\sim 10 \text{ nm}$ (Meyer-Vernet et al. 2009a), reproduced in Fig. 6. This measurement is compatible with

Fig. 8 Example of power spectrum measured with the X–Y dipole of STEREO/WAVES in the three low-frequency bands (*crosses*, acquisition times at *the top*). The two lower bands show dust impacts. The higher band (of much smaller acquisition time) detects only the plasma quasi-thermal noise

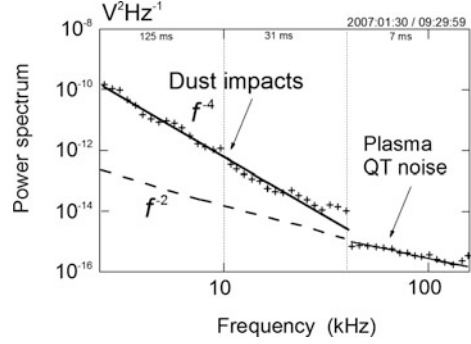
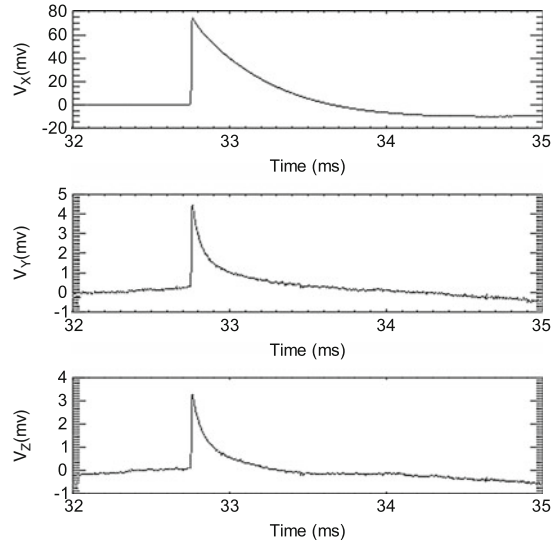


Fig. 9 Example of TDS pulse on the three monopoles upon a nanodust impact on STEREO A. The X antenna records a pulse (15) due to disruption of the antenna current balance (*top panel*), with a recoil due to instrumental filtering. The other antennas record a much smaller pulse (10) due to direct recollection of the cloud’s electrons by the spacecraft (*middle and bottom panels*). The decay times are close to the timescales of charge equilibrium restoration, for, respectively, an antenna and the spacecraft



the interplanetary dust model (Grün et al. 1985) and with the $m^{-5/6}$ collisional equilibrium (Dohnanyi 1969) curve which rawly approximates the flux at 1 AU for dust (except for the bump around 10^{-10} kg) and small bodies over more than 35 orders of magnitude in mass (Meyer-Vernet 2007).

Let us now check that the shape and amplitude of the voltage pulses observed with the three antennas agree in detail with our interpretation. Figure 9 shows an example of TDS data recorded on the three STEREO monopole antennas. The pulses are simultaneous (to the accuracy of the measurement \sim a few μ s), with $\delta V_y \sim \delta V_z \ll \delta V_x$, and the average observed ratio $\delta V_x / \delta V_y \simeq \delta V_x / \delta V_z \simeq 20$ (Zaslavsky et al. 2012). From the calculation of Sect. 2.3.4, one expects the antenna close to the impact location to record a pulse of large amplitude δV_2 given by (15) (top panel of Fig. 9) produced by disruption of the antenna current balance by the impact cloud, whereas the two other antennas record a pulse of much smaller

amplitude given by (10), produced by recollection of the cloud's electrons by the spacecraft. On STEREO, we have $L \simeq 6$ m, $R_{sc} \sim 1$ m, $n_a \sim 5 \text{ cm}^{-3}$, $C_{sc} \simeq 200$ pF, $\Gamma \simeq 0.5$, so that (10) and (15) yield

$$\delta V_2 \simeq [1.6 \times 10^{10} T_{\text{ph(eV)}}] Q, \quad (16)$$

$$\delta V_2 / \delta V_1 \simeq \frac{T_{\text{ph(eV)}} C_{sc}}{2\pi e n_a L R_{sc}^2} \simeq 6.6 T_{\text{ph(eV)}}. \quad (17)$$

From the observed value $\delta V_2 / \delta V_1 \simeq 20$, we deduce $T_{\text{ph}} \simeq 3$ eV, which is indeed the typical photoelectron temperature. Furthermore, a detailed study of the pulses detected on the three antennas during 4 years shows a striking agreement with the theoretical voltages expected from this interpretation (Zaslavsky et al. 2012).

Let us now examine whether the observed timescales also agree with this interpretation. First of all, let us verify that the observed rise time enables the antenna affected by the cloud to eject enough photoelectrons for producing the observed pulse amplitude. With a photoelectron current density $I_{\text{ph0}} \simeq 50 \mu\text{A}/\text{m}^2$ (Thiebault et al. 2006) and a projected surface area¹³ $\simeq 2ax \simeq 0.032x \text{ m}^2$ for the affected antenna length x , the charge accumulated during the observed rise time $\tau_r \sim 10\text{--}20 \mu\text{s}$ is $Q_{\text{ph}} \simeq I_{\text{ph0}} \times 2ax \times \tau_r \simeq [1.6 - 3.2]x \times 10^{-11} \text{ C}$. With the low-frequency monopole capacitance estimated in Sect. 2.3.4 yielding $C_A \simeq 64$ pF, this produces a pulse amplitude $\delta V_x \sim \Gamma Q_{\text{ph}} / C_A \sim [0.25 - 0.5] \Gamma x \text{ V}$, which is indeed close to the value given by (13).

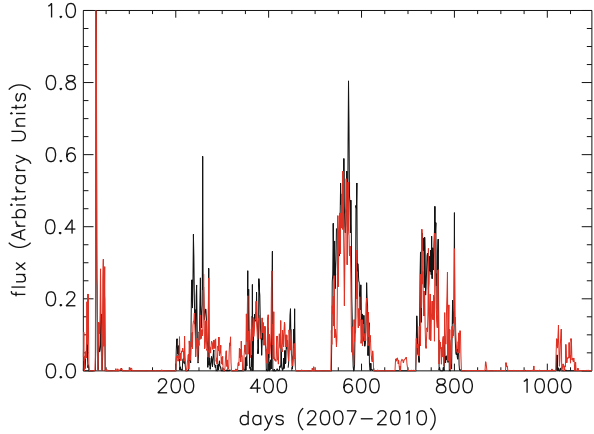
The decay of the pulses is governed by restoration of equilibrium by collection of solar wind electrons, which takes a much longer time ~ 1 ms (Fig. 9, top panel), of the order of magnitude of the theoretical equilibrium time of a STEREO antenna boom in the solar wind (Henri et al. 2011). Note that the pulses shown in the middle and bottom panels of Fig. 9, which are due to variation in spacecraft potential, decay faster since the equilibrium time of the spacecraft is shorter than that of an antenna by roughly the inverse ratio of their surface areas.

The power spectrum produced by averaging the impacts (Fig. 8) agrees with the shape given by (11). As we previously noted, it varies roughly as f^{-4} at frequencies greater than the inverse of the rise time, whereas the plasma noise due to impacts of ambient electrons varies roughly as f^{-2} for $f < f_p$ since the rise time is in that case $\sim 1/\omega_p$. Note that the STEREO antennas, of length $L = 6$ m, are too short compared to the solar wind Debye length $L_D \sim 10$ m to be able to detect a thermal noise peak at f_p , which explains why the plasma line does not appear in Figs. 2 and 8.

The evaluation based on the observed LFR spectra is affected by a large uncertainty because the relation (12) between the observed spectrum and the dust flux involves the rise time of the pulses, whose estimation is difficult. The TDS

¹³Since the antenna radius close to the antenna base is 1.6 cm (Bale et al. 2008).

Fig. 10 Nanodust fluxes (day-averages) in 2007–2010 from the TDS (TDS, in *red*) and the LFR (LFR band A, in *black*) on STEREO A. TDS data points are based on direct counting of impacts, whereas LFR data points are based on averages over the receiver acquisition time weighted according to the dust mass and speed (Sect. 2.3.4). Adapted from Zaslavsky et al. (2012)



instrument, which measures directly the individual pulses, reveals more information and has enabled us to refine the above estimate (Zaslavsky et al. 2012).

For a simplified illustration, let us use Fig. 7, which shows an example of TDS data recorded during a period of high dust impact rate, to evaluate the order of magnitude of the flux at this time. The sample exhibits four pulses during 130 ms, i.e., a cumulative flux $\sim 30 \text{ s}^{-1}$, for voltage amplitudes $> 20 \text{ mV}$. Converting voltages into charges with (16), and charges into masses with (2), assuming a nanodust speed $v \simeq 300 \text{ km/s}$ at 1 AU (Czechowski and Mann 2010, 2012), this yields $m > 3 \times 10^{-21} \text{ kg}$, for which the spacecraft surface for impacts affecting the antenna is from (6) $R_{\text{max}}^2 \sim 1 \text{ m}^2$. A correct calculation involving integration over the mass distribution as well as statistical averages (Zaslavsky et al. 2012) yields a similar order of magnitude for typical periods of high nanodust flux. However, the measured flux is extremely variable, both on small timescales—as illustrated in Fig. 2 which displays LFR data during 1 day, and on large timescales—as illustrated in Fig. 10 which shows the flux detected during 4 years with both TDS (in red) and LFR (in black).¹⁴

From the telemetered voltage samples acquired over 4 years (2007–2010) on STEREO A, we find a cumulative flux $F \sim 40 \text{ m}^{-2} \text{ s}^{-1}$ for the smaller mass $m \sim 3 \times 10^{-22} \text{ kg}$ (Zaslavsky et al. 2012). This flux is an overestimate since the TDS data selection is biased towards greater voltage amplitudes. The actual flux is smaller by an amount which depends on the statistics of the impacts and on the data selection process, and is at most the fraction of total telemetered time per day, i.e., a factor of 10^4 . This yields a cumulative flux for mass $3 \times 10^{-22} \text{ kg}$ (radius $\simeq 3 \text{ nm}$) in the range $0.4 \times [10^{-2} - 10^2] \text{ m}^{-2} \text{ s}^{-1}$ (Zaslavsky et al. 2012).¹⁵ These extreme values are

¹⁴Note that even in periods of very high flux, the number of impacts during the decay time $\tau_d \sim 1 \text{ ms}$ on the spacecraft surface affected by the impacts ($\sim R_{\text{max}}^2 \sim 1 \text{ m}^2$) never exceeds unity.

¹⁵The smaller value is deduced from the number of impacts detected during each day; it is a minimum value since the impacts are counted from about 50 samples (as the one shown in Fig. 7)

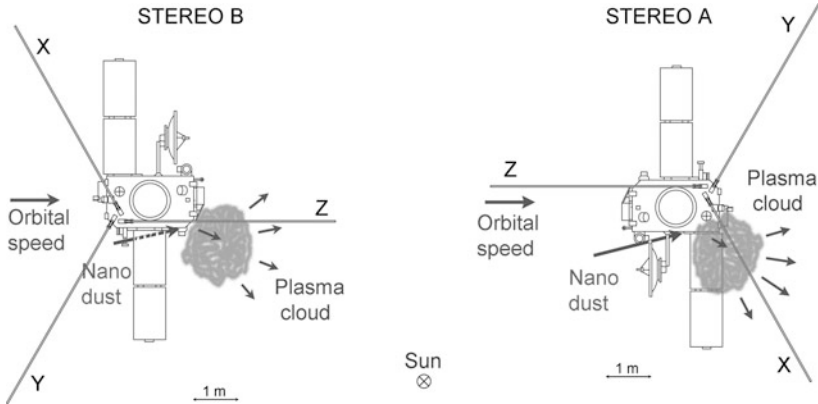


Fig. 11 The spacecraft STEREO A and B orbit the sun respectively ahead (A) and behind (B) the Earth. The views are from an observer looking towards the Sun. They show the three antenna booms X, Y, Z, with a tentative sketch of expanding plasma clouds produced by impacts of nanodust coming from the inner solar system and moving in the prograde sense

displayed in Fig. 6, together with dust models, and to the STEREO measurement of beta-particles, whose size is larger by two orders of magnitude.

As we already noted, the observed flux is highly variable on both short (seconds) and long (months) timescales. Impacts appear clearly in short bursts, but the observed long-term variability is different on STEREO A and B, as well as the antenna affected by the impact cloud (X on A, Z on B as labelled in Fig. 11), and the average impact rate, which is about twice lower on STEREO B than on STEREO A (Zaslavsky et al. 2012).

This large difference in long-term variability, with long periods of very low impact rate on STEREO A which are not observed on STEREO B, whereas the average fluxes on both spacecraft only differ by a factor of two and the short-term variability appears similar on both spacecraft, strongly suggests that a large part of the variability is due to changes in velocity direction of the particles, since both spacecraft have different attitudes, symmetrical with respect to the orbital speed, whereas the appendages such as solar panels—that prevent some spacecraft parts to be impacted from some directions—are positioned differently, as well as the antennas. Such changes in velocity direction may be associated to variations in solar wind properties that change the acceleration of the particles, whereas magnetic field variations at 0.1–0.2 AU from the Sun are expected to detrap nanodust from bound orbits, and enable them to be further accelerated by the solar wind (Czechowski and Mann 2012). Figure 11 illustrates the geometry, and sketches plasma clouds

of $\simeq 120$ ms each day, i.e., only 0.01% of each day, and the probability that no impact occurs during the rest of the day is extremely small. The higher value is deduced from the number of impacts detected during the telemetered time; it is a maximum value since the telemetered samples are not typical because the onboard data selection is biased towards greater voltage amplitudes.

produced by impacts of prograde nanodust coming from the inner solar system as predicted by dynamics (Czechowski and Mann 2010, 2012). This question is under study, as well as the time periodicities of the fluxes, the statistics of occurrence, and the dust mass distribution.

4 Detection of Jovian Nanodust with Cassini

After the STEREO/WAVES discovery of nanodust, the data from Cassini/RPWS were examined for possible nanodust signatures, even though the latter instrument is less adapted to this goal, for several reasons. First, the electric antennas are longer ($L = 10$ m) on Cassini than on STEREO, and they extend farther from the spacecraft, whose shape is quasi-cylindrical, which reduces the probability that the antenna current balance be affected by the impact clouds, in contrast to the quasi-flat surfaces of STEREO. Second, since the primary objective of Cassini was the study of Saturn's environment, it has furnished very few data at smaller heliocentric distances. Third, the waveforms used to detect individual dust impacts are either acquired with the antennas in dipole mode, or via the Langmuir probe which has a high noise level (Kurth et al. 2006).

Finally, the onboard algorithm used to select the waveforms to be transmitted on ground has a high effective threshold; for example, the sensitivity for detection of individual dust impacts in Saturn's E ring corresponds to grains of minimum radius $2.4 \mu\text{m}$ impacting at 8 km/s (Kurth et al. 2006). From (2), this is equivalent to grains of minimum radius 30 nm impacting at 300 km/s . Interplanetary dust of this size coming from the inner heliosphere are not expected to reach such a large speed (Czechowski and Mann 2012); furthermore, the average size of Jovian and Saturnian stream particles is smaller (Hsu et al. 2012). This suggests that the wide-band receiver on Cassini is not adapted to detect individual nanodust impacts.

In contrast, the high sensitivity of the hf receiver may enable it to detect fast nanodust if the impact rate is sufficiently high for (12) to yield a detectable power by integration over many impacts. An opportunity was offered by the Jovian flyby in December 2000–January 2001, when the Cosmic Dust Analysers on Cassini and Galileo made joint measurements of Jovian nanodust streams (Hsu et al. 2012) and revealed properties of the nanodust impacting Cassini (Graps et al. 2001), whereas the hf receiver of RPWS furnished data in both monopole and dipole mode. Figure 12 shows examples of power spectra acquired at this occasion in the jovian outer magnetosheath, which, from Sect. 2.3.4, correspond respectively to what is expected for nanodust impacts (left) and plasma quasi-thermal noise (right).

We can see in Fig. 13 that the large power corresponding to dust impacts is observed in monopole mode, with similar amplitudes on the different monopoles, the small difference being due to differences in antenna capacitances and receiver gains. This indicates that the signal is produced by recollection by the spacecraft of the impact-generated electrons, and not by perturbation of the current balance on an antenna. This is not surprising, because the photoelectron current at 5 AU is not large enough to produce a large voltage pulse when perturbed. Indeed, with

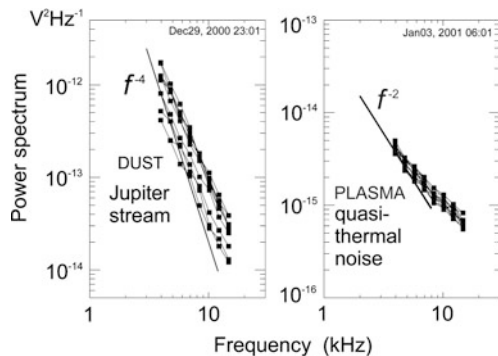


Fig. 12 Typical power spectra measured with the hf receiver on Cassini/RPWS near Jupiter. The *left* and *right spectra* are produced respectively by nanodust impacts and by the plasma quasi-thermal noise (with antennas smaller than the plasma Debye length). Adapted from Meyer-Vernet et al. (2009b)

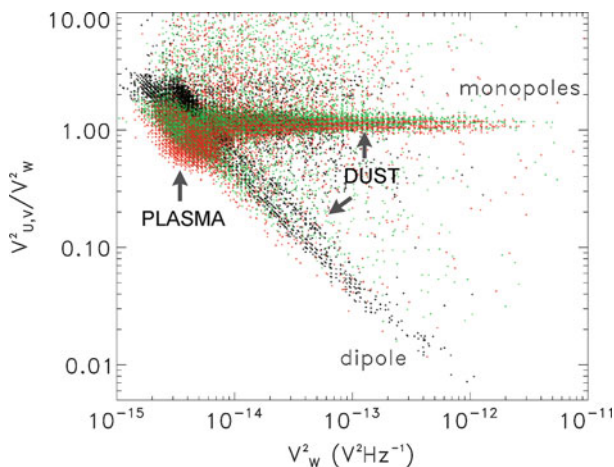


Fig. 13 Cassini/RPWS hf receiver data near Jupiter. Ratios of the power on two monopoles (*red* and *green*) to that on the other one as a function of the latter, and ratio of the power on the dipole to that on the monopole (*black*). The dust yields similar signals on the monopoles, whereas the dipole records mainly the plasma thermal noise (of smaller amplitude). From Meyer-Vernet et al. (2009b)

$a = 1.43 \text{ cm}$ (Gurnett et al. 2004), $T_{\text{ph}} \simeq 3 \text{ eV}$, $I_{\text{ph}0} \simeq 2 \times 10^{-6} \mu\text{A m}^{-2}\text{s}^{-1}$ at 5 AU and τ given by the pulse rise time $\tau_r \simeq 40 \mu\text{s}$ deduced from the observed spectral shape, condition (14) does not hold.

Estimating Q from (2), with the particles properties $m \simeq 10^{-21} \text{ kg}$, and $v \simeq 450 \text{ km/s}$ deduced from the Cassini/Galileo joint measurements (Graps et al. 2001), we use (10)–(12) to deduce the relation between the power spectral density on the Cassini RPWS monopoles and the dust flux F (Meyer-Vernet et al. 2009b)

$$V^2 \simeq 1.5 \times 10^{-11} F / f_{(\text{kHz})}^4 \text{ V}^2\text{Hz}^{-1} \tag{18}$$

From the measured power spectral density (see for example Fig. 12, left) we find the maximum flux $F \sim 10 \text{ m}^{-2} \text{ s}^{-1}$ in the streams on December 30, 2000, with a time variation similar to that measured by the CDA. This flux is also in the range of values reported by long-term studies of jovian dust streams with Galileo, both in amplitude and variability (Krüger et al. 2005).

5 Conclusions and Perspectives

Contrary to the nanodust wave detection performed with Cassini near Jupiter, which was a mere confirmation of results obtained with classical detectors, the nanodust seen by STEREO at 1 AU had never been observed before. Even though these observations had been predicted theoretically and are compatible with the interplanetary dust model, it is therefore especially important to check their validity. First of all, the possibility that the signals are generated or affected by internal noise or electromagnetic interferences has been eliminated. Numerous tests had been made before and after launch to make sure that the spacecraft was extremely clean and that the instrument was not significantly perturbed by other instruments nor by spacecraft subsystems. Possible remaining perturbations have been carefully eliminated from the data, as well as voltages generated by other radio or plasma wave phenomena or impacts of energetic particles. Second, the observations are made with two independent subsystems of the instrument (LFR and TDS), which yield compatible results (Meyer-Vernet et al. 2009a; Zaslavsky et al. 2012). Third, the instrument also detects other kinds of dust, yielding results that agree with previous measurements by classical dust detectors (Zaslavsky et al. 2012). Finally, the interpretation of the data in terms of voltage pulses produced by impact ionisation explains the amplitude and shape of the observed pulses and the different responses of the antennas, using only known concepts.

However, since nanodust detections with wave experiments have been performed serendipitously, with instruments that were not designed for this purpose, the error bars are presently large, and since these measurements took place very recently, the mechanism of detection and the calibration for dust measurements are still under study. More specifically, the following items are still being investigated. First, a major problem is the use of calibrations such as the charge production described in (2). Not only are they not specific to these instruments, but they rely on laboratory experiments performed with dust grains that are both larger and slower. Specific calibrations should be performed on future instruments. Second, the mechanism of electric field production must be investigated in more detail. This requires a more detailed study of the observed shape of the pulses, as well as a complex simulation taking into account the geometry and environment of the spacecraft and antennas. Finally, the flux variability is being investigated from short (~ 1 s) to large (years) timescales, in comparison to the solar wind state, as well as the mass distribution, especially near the low end of the mass range. This latter question is of great importance, since no lower size cut-off has presently been detected in

the interplanetary dust distribution, and the properties of these particles lying at the frontier between molecules and bulk matter are badly known, as well as their interactions with the solar wind.

Other data are under study. A number of events suggesting nanodust impacts detected on Cassini/RPWS at heliocentric distances between 1 and 3 AU are being investigated. Few similar events have been detected at farther heliocentric distances and in Saturn environment, and they are much weaker. This is not surprising for several reasons. We have seen that the RPWS waveform mode is not adapted for detecting nanodust impacts, whereas the hf receiver requires a large impact rate to yield a detectable power. Furthermore, the particles produced at Saturn are smaller and slower than those produced at Jupiter (Hsu et al. 2012), and are therefore expected to yield a smaller signal, and furthermore the very small photoelectron current at Jupiter and Saturn distances is not expected to perturb sufficiently the antenna current balance.

Wave data from other interplanetary probes are also being investigated. As a rule, they are not adapted for nanodust detection because they were designed for radio observations, so that they use long antennas extending far from the spacecraft and operated in dipole mode. The length of the antennas and their very small radius imply that the plasma clouds produced by impacts on the spacecraft are not expected to disturb significantly the photoelectrons that control the current balance on antennas and therefore to produce a pulse detectable in dipole mode; for example, with the 2×45 m electric antennas on the spacecraft WIND, (15) yields a pulse amplitude smaller than the value on STEREO by nearly one order of magnitude, and anyway, the antenna radius $a \simeq 0.2$ mm is too small for condition (14) to hold. Recollection of impact electrons by the spacecraft cannot be detected either since the antennas are operated in dipole mode.

The question arises as to whether the radio experiment on Ulysses detected nanodust, especially when the Cosmic Dust Analyser did so near Jupiter in 1992 (Krüger et al. 2006). The radio experiment on Ulysses (Stone et al. 1992) does not have a TDS, but it has an antenna operated in monopole mode, and some low frequency signals have indeed been detected at the times when the CDA detected nanodust impacts near Jupiter in 1992. However, the signals are difficult to analyse because this LFR of old generation is swept through the different frequency channels, doing so in about 2 min. Since STEREO results show that the dust impact rate may vary considerably during this time, this means that a characteristic dust spectrum cannot be observed, since each frequency channel acquired at a different time observes a different impact rate. Furthermore, there is no TDS mode in order to measure the shape of the pulses.

Another major point is the question of the origin of the interplanetary nanodust discovered by STEREO. The main source is expected to be the inner solar system, as proposed by Czechowski and Mann (2010, 2012). A Jovian origin of the particles is clearly excluded, except occasionally, since the average flux measured by the Cosmic Dust Analyser as a function of Jovicentric distance (Krüger et al. 2006) would yield a flux at 4 AU from Jupiter much smaller than the average flux observed by STEREO during 4 years.

On the other hand, a contribution from the Earth environment is not presently excluded. Estimating this contribution requires a calculation of the ejection speed (if any) from the Earth, from which the dust would be accelerated by the solar wind. This calculation is not simple because of the complex Earth's environment in which the dust charge varies during its motion. The fact that the charge is expected to be negative in most of the plasmasphere, i.e., inward of the synchronous orbit, and generally positive outward because of the smaller plasma density, except in shadow (Horányi et al. 1988) might enable outward acceleration by the corotation electric field as in outer planets, albeit to smaller speeds since the magnetic field, rotation rate, and radius are smaller. Assuming that the main forces on nanodust are the corotation electric force and gravitation, a necessary condition for ejection of a charge q of mass m from a Keplerian orbit of radius r_0 (assumed significantly smaller than the magnetospheric size) is that the corotation potential $\Phi \simeq q\Omega_{\oplus}B_{\oplus}R_{\oplus}^3/r_0$ (Burns et al. 2001) exceeds the energy $mM_{\oplus}G/2r_0$. Here Ω_{\oplus} , B_{\oplus} , R_{\oplus} are, respectively, the Earth's angular rotation frequency, equatorial magnetic field, and radius. Substituting the Earth properties, this condition yields $q/m > 3 \times 10^{-6}e/m_p$. With a grain's electrostatic potential $\phi \sim 10$ V and mass density $\simeq 2.5 \times 10^3 \text{ kg m}^{-3}$, this translates into a grain radius $r < 20$ nm. This necessary condition is generally not sufficient since too small grains, of gyroradius smaller than the scale of magnetic variation, are expected to be confined along magnetic field lines. However, the Earth's magnetosphere undergoes frequent perturbations which disrupt the magnetic lines and may enable ejection of these grains, especially along the magnetic tail. Even though a first examination of the data did not show any simple correlation between the observed impact rate and geomagnetic perturbations, which is not surprising since most of the dust acceleration is expected to take place in the solar wind and may confine the grains in narrow streams, a more detailed study is in progress.

Finally, these observations enable one to derive some consequences for the design of wave experiments for measuring dust on future instruments such as RPW on Solar Orbiter and FIELDS on Solar Probe Plus. Solar Orbiter will explore the heliosphere on an elliptic orbit with a perihelion as low as 0.28 AU and increasing inclination up to more than 30° with respect to the solar equator. Solar Probe Plus will explore the solar corona as close as 9.5 solar radii.

In order to optimise the measurements, instrumental modes specifically dedicated to dust detection are currently under development. This may include a specific frequency receiver without AGC, and a TDS mode performing a systematic detection and recording of the nanodust impact main properties, thereby greatly reducing the uncertainties due to the biased event selection of the existing TDS. The realisation of ground-based experiments in dust accelerators is also under study. The aim is to measure the charge Q generated by an impact on the actual spacecraft surface materials, and to perform a ground calibration of the radio detection technique, in order to better understand the processes at the origin of the observed electric signals.

References

- Aubier, M., Meyer-Vernet, N., Pedersen, B.M.: 1983, *Geophys. Res. Lett.* **10**, 5.
- Auer, S.: 2001, In: Grün, E. et al. (eds.) *Interplanetary dust*, Springer, 385.
- Bale, S.D., Ullrich, R., Goetz, K., Alster, N., Cecconi, B., Dekkali, M. et al.: 2008, *Space Sci. Rev.* **136**, 487.
- Bird, R.S., McKee, L.L., Schwirzke, F., Cooper, A.W.: 1973, *Phys. Rev. A* **7**, 1328.
- Bougeret, J.-L., Goetz, K., Kaiser, M.L., Bale, S.D., Kellogg, P.J., Maksimovic, M. et al.: 2008, *Space Sci. Rev.* **136**, 529.
- Burns, J.A., D.P. Hamilton, M.R. Showalter: 2001, In: Grün, E. et al. (eds.) *Interplanetary dust*, Springer, 641.
- Ceplecha, Z., Borovicka, J., Elford, W.G., Revelle, D.O., Hawkes, R.L., Porubcan, V. et al.: 1998, *Space Sci. Rev.* **84**, 327.
- Czechowski, A., Mann, I., : 2010, *Astrophys. J.* **714**, 89.
- Czechowski, A., Mann, I., : 2012, this volume.
- Davis, C.J., Davies, J.A., St Cyr, O.C., Campbell-Brown, M., Skelt, A., Kaiser, M. et al.: 2012, *Mon. Not. Roy. Astron. Soc.*, **420**, 1355
- Dietzel, H., Eichhorn, G., Fechtig, H., Grün, E., Hoffmann, H.-J., Kissel, J.: 1973, *J. Phys. E. Scientif. Instr.* **6**, 209.
- Dohnanyi, J.S.: 1969, *J. Geophys. Res.* **74**, 2531.
- Drapatz, S. and Michel, K.W.: 1974, *Z. Naturforsch.* **29a**, 870.
- Driesman, A., Hynes, S., Cancro, G.: 2008, *Space Sci. Rev.* **136**, 17.
- Foschini, L.: 1998, *Europhys. Lett.* **43**, 226.
- Göller, J.R., Grün, E.: 1989, *Planet. Space Sci.* **37**, 1197.
- Graps, A.L., E. Grün, H. Krüger, M. Horányi, and H. Svedhem: 2001, In: Warmbein, B. (ed.) *Proceed. Meteor. 2001 Conf.*, ESA **SP-495**, ESTEC, Noordwijk, 601–608.
- Grün, E., Zook, H.A., Fechtig, H., Giese, R.H.: 1985, *Icarus* **62**, 244.
- Grün, E. et al.: 1992, *Science* **257**, 1550.
- Grün, E., Baguhl, M., Svedhem, H., Zook, H.A.: 2001, In: Grün, E. et al. (eds.) *Interplanetary dust*, Springer, 295.
- Gurnett, D.A., Grün, E., Gallagher, D., Kurth, W.S., Scarf, F.L.: 1983, *Icarus* **53**, 236.
- Gurnett, D.A., Kurth, W.S., Kirchner, D.L., Hospodarsky, G.B., Averkamp, T.F., et al.: 2004, *Space Sci. Rev.*, 114, 395–463.
- Henri, P. et al.: 2011, *Physics of Plasmas*, **18**, 082308.
- Horányi, M., H.L.F. Houpis, D.A. Mendis: 1998, *Astrophys. Space Sci.*, **144**, 215.
- Horányi, M., E. Grün, and A. Heck: 1997, *Geophys. Res. Lett.*, **24**, 2175–2178.
- Hornung, K., Kissel, J.: 1994, *Astron. Astrophys.* **291**, 1.
- Hornung, K., Malama, Y., G., Kestenboim, K.S.: 2000, *Astrophys. Space Sci.* **274**, 355.
- Hsu, W.H., Krüger, H., Postberg, F.: 2012, this volume.
- Johnson, T. V., G. Morfill, and E. Grün: 1980, *Geophys. Res. Lett.*, **7**, 305–308.
- Kissel, J., Krüger, F.R.: 1987, *Appl. Phys. A* **42**, 69.
- Krüger, F.R.: 1996, *Adv. Space Res.* **17**, 1271.
- Krüger, H., Linkert, G., Linkert, D., Moissl, R., and Grün, E.: 2005, *Planet. Space Sci.*, **53**, 1109.
- Krüger, H., Graps, A.L., Hamilton, D.P., Flandes, A., Forsyth, R.J., Horanyi, M., Grün, E.: 2006, *Planet. Space Sci.*, **54**, 919.
- Kurth, W.S., T.F. Averkamp, D.A. Gurnett, and Z. Wang: 2006, *Planet. Space Sci.*, **54**, 988.
- Mann, I., Murad, E., Czechowski, A.: 2007, *Planet. Space Sci.* **55**, 1000.
- Mann, I., Czechowski, A., Meyer-Vernet, N., Zaslavsky, A., Lamy, H.: 2010, *Plasma Physics and Controlled Fusion* **52**, 124012.
- Mann, I., Pellinen-Wannberg, A., Murad, E., Popova, O. et al.: 2011, *Space Sci. Rev.*, **36**.
- Manning, R.: 1998, In: Pfaff, R. et al. (eds.) *Measurement techniques in Space Plasmas: Fields*, *Geophys. Monograph Ser.* **103**, AGU, Washington DC., 181.
- McBride, N., McDonnell, J.A.M.: 1999, *Planet. Space Sci.* **47**, 1005.

- Meuris, P. et al.: 1996, *J. Geophys. Res.* **101**, 24471.
- Meyer-Vernet, N.: 1979, *J. Geophys. Res.* **84**, 5373.
- Meyer-Vernet, N.: 1985, *Adv. Space Res.* **5**, 37.
- Meyer-Vernet, N.: 2001, In: Harris, R. A. (ed.), *Proc. 7th Spacecraft Charging Technology Conf.*, ESA SP-476, Noordwijk: ESTEC, 635.
- Meyer-Vernet, N.: 2007, *Basics of the Solar Wind*, Cambridge University Press, 339, 351–355.
- Meyer-Vernet, N., Perche, C.: 1989, *J. Geophys. Res.* **94**, 2405.
- Meyer-Vernet, N., Aubier, M.G., Pedersen, B.M.: 1986, *Geophys. Res. Lett.* **13**, 617.
- Meyer-Vernet, N., A. Lecacheux, and B.M. Pedersen: 1996, *Icarus*, 123, 113.
- Meyer-Vernet, N., S. Hoang, K. Issautier, M. Maksimovic, R. Manning, M. Moncuquet, R. Stone: 1998, In: Pfaff, R. et al. (eds.) *Measurement techniques in Space Plasmas: Fields, Geophys. Monograph Ser.* **103**, AGU, Washington DC., 205.
- Meyer-Vernet, N., Maksimovic, M., Czechowski, A., Mann, I., Zouganelis, Z., Goetz, K. et al.: 2009a, *Solar Phys.* **256**, 463.
- Meyer-Vernet, N., Lecacheux, A., Kaiser, M.L., Gurnett, D.A.: 2009b, *Geophys. Res. Lett.* **36**, L03103.
- Oberc, P.: 1994, *Icarus* **111**, 211.
- Oberc, P.: 1996, *Adv. Space Res.* **17**, (12)105.
- Oberc, P., Parzydło, W., Vaisberg, O.L.: 1990, *Icarus* **86**, 314.
- Pantellini, F., Landi, S., Zaslavsky, A., Meyer-Vernet, N.: 2012a, *Plasma Physics and Controlled Fusion*, in press.
- Pantellini, F. et al.: 2012b, *Astrophys. Space Sci.*, **54**, 045005
- Pedersen, B. et al.: 1991, *J. Geophys. Res.* **96**, 19187.
- Scarf, F.L., D.A. Gurnett, W.S. Kurth, and R.L. Poynter: 1982, *Science*, **215**, 587.
- Shanbing, Y., S. Gengchen, T. Qingming: 1994, *Int. J. Impact Engng*, **15**, 67.
- Stamper, J.A., Papadopoulos, K., Sudan, R.N., Dean, S.O., Mclean, E.A.: 1971, *Phys. Rev. Lett.* **26**, 1012.
- Stone, R.G., Pedersen, B.M., Harvey, C.C., Canu, P., Cornilleau-Wehrin, N., Desch, M.D. et al.: 1992, *Science*, **257**, 1524.
- St. Cyr, O.C., Kaiser, M.L., Meyer-Vernet, N., Howard, R.A., Harrison, R.A., Bale, S.D. et al.: 2009, *Solar Phys.*, **256**, 475.
- Thiebault, B., Hilgers, A., Masson, A., Escoubet, C.P., Laakso, H.: 2006, *IEEE Trans. Plasma Sci.* **34**, 2078.
- Warwick, J. W. et al.: 1982, *Science*, 215, 582–586.
- Zaslavsky, A., Meyer-Vernet, N., Hoang, S., Maksimovic, M., Bale, S. D.: 2011, *Radio Sci.*, **46** (2), doi: 10.1029/2010RS004464.
- Zaslavsky, A., Meyer-Vernet, N., Mann, I., Czechowski, A., Issautier, K., Le Chat, G. et al.: 2012, *J. Geophys. Res.*, in press.
- Zook, H. A., Grün, E., Baguhl, M., Hamilton, D.P., Linkert, G., Liou: 1996, *Science* **274**, 1501.